

Initializing ReLU networks in an expressive subspace of weights

Dayal Singh¹ and G J Sreejith¹

¹Indian Institute of Science Education and Research, Pune 411008, India.

Abstract

Using a mean-field theory of signal propagation, we analyze the evolution of correlations between two signals propagating through a ReLU network with correlated weights. Signals become highly correlated in deep ReLU networks with uncorrelated weights. We show that ReLU networks with anti-correlated weights can avoid this fate and have a chaotic phase where the correlations saturate below unity. Consistent with this analysis, we find that networks initialized with anti-correlated weights can train faster (in a teacher-student setting) by taking advantage of the increased expressivity in the chaotic phase. Combining this with a previously proposed strategy of using an asymmetric initialization to reduce dead ReLU probability, we propose an initialization scheme that allows faster training and learning than the best-known methods.

1 Introduction

Rectified Linear Unit (ReLU) [1, 2] is the most widely used non-linear activation function in Deep Neural Networks (DNNs) [3, 4, 5], applied to various tasks like computer vision [6, 7, 8], speech recognition [9, 10, 11], intelligent gaming [12], and solving scientific problems [13]. ReLU, $\phi(x) = \max(0, x)$, outperforms most of the other activation functions proposed [14]. It has several advantages over other activations. ReLU activation function is computationally simple as it essentially involves only a comparison operation. ReLU suffers less from the vanishing gradients, a major problem in training networks with sigmoid-type activations that saturate at both ends [6]. They generalize well even in the overly parameterized regime [15].

Despite its success, ReLU also has a few drawbacks, one of which is the dying ReLU problem [8, 16]. The dying ReLU is a type of vanishing gradient problem in which the network outputs zero for all inputs and is dead. There is no gradient flow in this state. ReLU also suffers from exploding gradient problem, which occurs when backpropagating gradients become large [17].

Several methods are proposed to overcome the vanishing/exploding gradient problem; these can be classified into three categories [18]. The first approach modifies the architecture, which includes using modified activation functions [4, 8, 16, 19, 20, 21], adding connections between non-consecutive layers (residual connections)[22], and optimizing network depth and width. The proposed activations are often computationally less efficient and require a fine-tuned parameter [18]. The second approach relies on normalization techniques [23, 24, 25, 26, 27], the most popular one being batch normalization [24]. Batch normalization prevents the vanishing and exploding gradients by normalizing the output at each layer but with an additional computational cost of up to 30% [28]. A related strategy involves using the self-normalizing activation (SeLU), which by construction ensures output with zero mean and unit variance [20]. The third approach focuses on the initialization of the weights and biases. As local (gradient-based) algorithms are used for

optimization [29, 30, 31], it is challenging to train deep networks with millions of parameters [32, 33], and optimal initialization is essential for efficient training [34]. He-initialization [8] is a commonly used strategy. Recently, Ref. [18] proposed Random Asymmetric initialization (RAI), which reduces the probability of dead ReLU at the initialization. In this paper, we aim to improve the initialization scheme for ReLU networks.

A growing body of work has analyzed signal propagation in infinitely wide networks to understand forward-propagation in DNNs, [35, 36, 37, 38, 39, 40, 41, 42, 43]. We mention a few results for ReLU networks. Ref. [40] showed that correlations in input signals propagating through a ReLU network always converge to one. Many other works found that ReLU networks are biased towards simpler functions [44, 45, 46, 47, 48], which may account for their better generalization properties even in the overly parameterized regime. However, from their successful application in different domains, one may guess that they should be capable of computing more complex functions. There might be a subspace of the parameters where the network can represent complex functions.

Ref. [41, 42] applied weight and input perturbations to analyze the function space of ReLU networks. They found that ReLU networks with anti-correlated weights explore the function space farther than uncorrelated/positively correlated weights. Ref. [49] found that ReLU CNN’s produce anti-correlated feature matrices after training. These two studies motivated us to analyze the critical properties of signal propagation in anti-correlated ReLU networks.

Following the mean-field theory of signal propagation proposed by Ref. [36], we found that ReLU networks with anti-correlated weights have a chaotic phase, which implies higher expressivity. In contrast, ReLU networks with uncorrelated weights do not have a chaotic phase. We find that initializing ReLU networks with anti-correlated weights results in faster training. We call it Anti-correlated initialization (ACI). Further improvement in performance is achieved by incorporating RAI, which reduces the dead ReLU probability. This combined scheme, which we call Random anti-correlated asymmetric initialization (RAAI) is the main result of this work, and is defined as follows. We pick weights and bias incoming to a neuron from anti-correlated Gaussian distribution (like Eqn. 2) and replace a randomly picked weight/bias with a random variable drawn from a beta distribution. The code to generate weights drawn from the RAAI distribution is given in Appendix E. We analyze the correlation properties of RAAI and show that it performs better than the best-known initialization schemes on tasks of varying complexity. It may be of concern that initialization in an expressive space may lead to overfitting, and we do observe the same for ACI for deeper networks and complex tasks. In contrast RAAI shows no signs of overfitting and performs consistently better than all other initialization schemes.

We organize the article as follows: First, we review the mean-field theory of signal propagation in Section 2. Next, in Section 3, we analyze signal propagation with correlated weights. Section 4 describes the various tasks used to validate the performance of different initialization schemes. In Section 5, we study the dynamics and performance of ReLU networks initialized with anti-correlated weights. Section 6 analyzes the critical properties of correlations in input signals for RAI and RAAI. Next, Section 7 compares different initialization schemes, and lastly, Section 8 concludes the article.

2 Mean-field analysis of signal propagation

We begin by reviewing a mean-field approach proposed by Ref. [36, 38] to analyze signal propagation through infinitely wide neural networks. For an alternative derivation using generating functionals, see Ref. [41].

Consider a fully connected neural network with L layers with N_l neurons in layer l . For an

input signal x , we denote the pre-activation at node i in layer l by $h_i^l(x)$, and activation by $s_i^l(x)$. A signal $(s_1^{l-1}, \dots, s_{N_l}^{l-1})$ at layer $l-1$ propagates to layer l by the rule

$$h_i^l(x) = \sum_{j=1}^{N_{l-1}} w_{ij}^l s_j^{l-1}(x) + b_i^l$$

$$s_i^l(x) = \phi(h_i^l(x)),$$

where ϕ is the non-linear activation function and $w_{ij}^l \sim \mathcal{N}(0, \frac{\sigma_w^2}{N_{l-1}})$, $b_i^l \sim \mathcal{N}(0, \sigma_b^2)$ are the weights and biases. The $1/N_{l-1}$ scaling in the weight's variance ensures that the input contribution from the last layer to each neuron is $\mathcal{O}(1)$.

To track the layer-wise information flow, consider the normalized length and overlap of the pre-activations for two input signals x_1, x_2 , reaching layer l

$$q_h^l(x_a) = \frac{1}{N_l} \sum_{i=1}^{N_l} \left(h_i^l(x_a) \right)^2 \text{ where } a \in \{1, 2\}$$

$$q_h^l(x_1, x_2) = \frac{1}{N_l} \sum_{i=1}^{N_l} h_i^l(x_1) h_i^l(x_2).$$

The covariance matrix between the signals is obtained by performing appropriate averages of q_h^l over input signals.

Assuming self averaging, consider an average over all possible networks, i.e., the weights and biases. For simplicity of notations later, we use the same symbol for averaged q_h^l .

$$q_h^l(x_a) = \frac{1}{N_l} \left\langle \sum_{i=1}^{N_l} \left(h_i^l(x_a) \right)^2 \right\rangle = \sum_{j,k=1}^{N_{l-1}} \langle w_{ij}^l w_{ik}^l \rangle \phi(h_j^{l-1}(x_a)) \phi(h_k^{l-1}(x_a)) + \langle (b_i^l)^2 \rangle,$$

$$q_h^l(x_1, x_2) = \frac{1}{N_l} \left\langle \sum_{i=1}^{N_l} h_i^l(x_1) h_i^l(x_2) \right\rangle = \sum_{j,k=1}^{N_{l-1}} \langle w_{ij}^l w_{ik}^l \rangle \phi(h_j^{l-1}(x_1)) \phi(h_k^{l-1}(x_2)) + \langle (b_i^l)^2 \rangle,$$

where $\langle \cdot \rangle$ denotes an average over the weights and biases. Since the weights and biases are uncorrelated, we obtain

$$q_h^l(x_a) = \frac{\sigma_w^2}{N_{l-1}} \sum_j \left(\phi(h_j^{l-1}(x_a)) \right)^2 + \sigma_b^2$$

$$q_h^l(x_1, x_2) = \frac{\sigma_w^2}{N_{l-1}} \sum_j \phi(h_j^{l-1}(x_1)) \phi(h_k^{l-1}(x_2)) + \sigma_b^2.$$

For large N_l , each h_i^l is a weighted sum of uncorrelated random variables. Thus, we expect the distribution of $h_i^l(x_1), h_i^l(x_2)$ to converge to a zero-mean Gaussian with a covariance matrix given by

$$\Sigma_h^{l-1}(x_1, x_2) = \begin{bmatrix} q_h^{l-1}(x_1) & q_h^{l-1}(x_1, x_2) \\ q_h^{l-1}(x_1, x_2) & q_h^{l-1}(x_2) \end{bmatrix}.$$

On replacing the average over nodes by Gaussian distribution with appropriate covariance, we obtain iterative maps for the length and overlap

$$\begin{aligned} q_h^l(x) &= \mathcal{V}\left(q_h^{l-1}(x) \mid \sigma_w^2, \sigma_b^2\right) \\ q_h^l(x_1, x_2) &= \mathcal{C}\left(c_h^{l-1}(x_1, x_2), q_h^{l-1}(x_1), q_h^{l-1}(x_2) \mid \sigma_w^2, \sigma_b^2\right), \end{aligned} \quad (1)$$

where the map \mathcal{V} is given by

$$\mathcal{V}\left(q_h^{l-1}(x) \mid \sigma_w^2, \sigma_b^2\right) = \sigma_w^2 \int Dz \phi\left(\sqrt{q_h^{l-1}(x)} z\right)^2 + \sigma_b^2,$$

and the map \mathcal{C} is given by

$$\begin{aligned} \mathcal{C}\left(c_h^{l-1}(x_1, x_2), q_h^{l-1}(x_1), q_h^{l-1}(x_2) \mid \sigma_w^2, \sigma_b^2\right) &= \sigma_w^2 \int Dz_1 Dz_2 \phi(u_1) \phi(u_2) \\ u_1 &= \sqrt{q_h^{l-1}(x_1)} z_1, \quad u_2 = \sqrt{q_h^{l-1}(x_2)} \left[c_h^{l-1}(x_1, x_2) z_1 + \sqrt{1 - (c_h^{l-1}(x_1, x_2))^2} z_2 \right]. \end{aligned}$$

Here $c_h^l(x_1, x_2) = q_h^l(x_1, x_2) / \sqrt{q_h^l(x_1) q_h^l(x_2)}$ is the correlation coefficient between the two signals reaching layer l , and Dz is the standard Gaussian measure.

Ref. [36] found that the signal's length reaches its fixed point within very few layers, and the fixed point of the correlation coefficient, $c_h^*(x_1, x_2)$, can be estimated with the assumption that $q_h^l(x)$ has reached its fixed point $q^*(x)$. It is easy to see that $c_h^*(x_1, x_2) = 1$ is always a fixed point of the dynamics. The stability of the fixed point $c_h^*(x_1, x_2) = 1$ is determined by

$$\chi_1 \equiv \frac{\partial c_h^l(x_1, x_2)}{\partial c_h^{l-1}(x_1, x_2)} \Big|_{c_h^{l-1}(x_1, x_2)=1} = \sigma_w^2 \int Dz [\phi'(\sqrt{q^*(x)} z)]^2.$$

χ_1 separates the dynamics into two phases - first, an ordered phase with $\chi_1 < 1$, where the $c_h^*(x_1, x_2) = 1$ fixed point is stable; and second, a 'chaotic' phase with $\chi_1 > 1$, where the $c_h^*(x_1, x_2) = 1$ fixed point is unstable. $\chi_1 = 1$ defines the phase boundary line. In the ordered phase, two distinct signals will become perfectly correlated asymptotically. In the chaotic phase, the correlations converge to a stable fixed point below unity. In this phase, even two closely related signals will eventually lose correlations. Initializing the network with parameters (σ_w^2, σ_b^2) at the phase transition boundary (corresponding to an infinite depth of correlations) allows for an optimal information flow through the network.

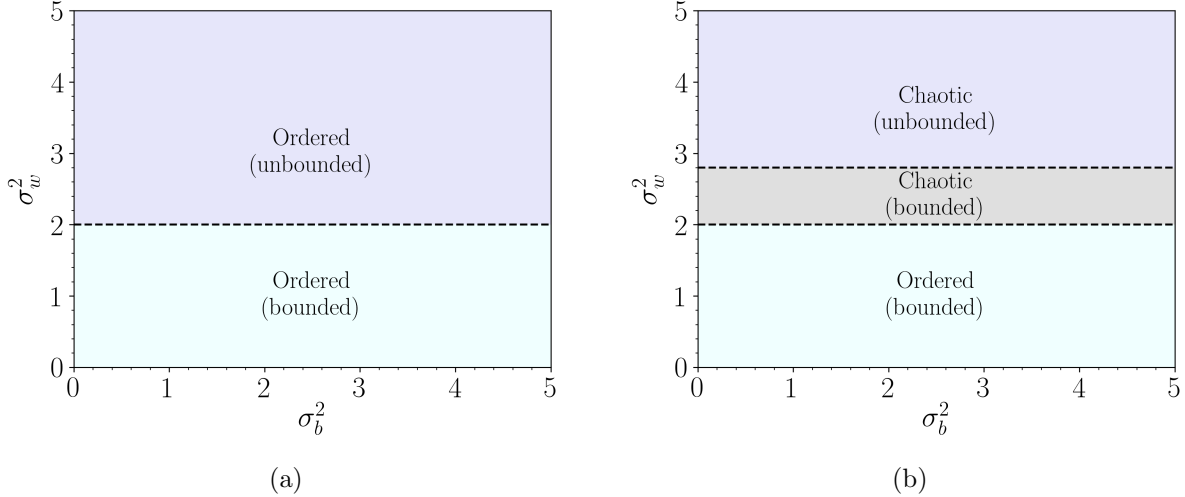


Figure 1: Phase diagram for ReLU networks with uncorrelated and anti-correlated Gaussian distributed weights. (a) ReLU networks with uncorrelated weights have two phases. First, a bounded phase where $q^*(x)$ is finite, and second in which it diverges. The two phases are separated by $\sigma_w^2 = 2$. In both phases, any two signals will eventually become correlated (b) ReLU networks with anti-correlated weights have three phases. In addition to the phase boundary for the length (at some $\sigma_w^2 > 2$), there exists a phase transition for the correlation coefficient at $\sigma_w^2 = 2$.

The discussion so far in this section applies to a general non-linear activation ϕ . Now we will focus on the case of ReLU activation. The above analysis is applied assuming $q^*(x)$ is finite shows that ReLU networks do not have a chaotic phase, and any two signals propagating through a ReLU network become asymptotically correlated for all values of (σ_w^2, σ_b^2) . In other words, $c^*(x_1, x_2) = 1$ is always a stable fixed point in the regime where signal strength is bounded.

The parameter space of the network can be classified into two phases based on the boundedness of the fixed point $q^*(x)$ of the length map (Eqn. 1) - first, a bounded phase where $q^*(x)$ is finite and non-zero; second, an ‘unbounded’ phase, where $q^*(x)$ is either zero or infinite [39, 50]. Fig. 1a depicts the phase diagram for ReLU networks. The two phases are separated by the boundary $\sigma_w^2 = 2$. Initializing ReLU networks with $(\sigma_w^2, \sigma_b^2) = (2, 0)$ is commonly known as He initialization [8]. The analysis of the stability of $c^*(x_1, x_2) = 1$ fixed point in ReLU networks is valid only in the bounded phase. Numerical results presented below indicate that the fixed point remains stable even in the unbounded phase.

In Fig. 2, we show the values of the length and correlation coefficient as a function of the variance of weights after uncorrelated signals have propagated through l layers. The above quantities were calculated by first averaging over $M = 1024$ input signals, then averaging over 40 networks initialized with independently picked $w_{ij}^l \sim \mathcal{N}(0, \sigma_w^2/N)$, where we have considered a constant width $N_l = N = 2048$. We observe the results as predicted by Eqn. 1. The signal’s length starts to diverge at $\sigma_w^2 = 2$, and the correlation coefficient after propagation through 32 layers is almost one.

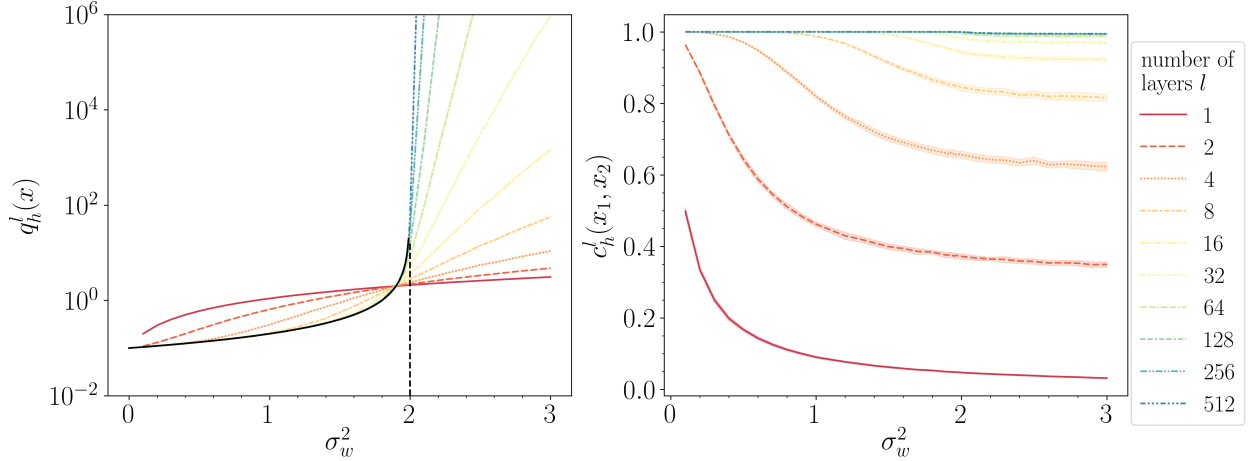


Figure 2: The above plots show the length and the correlation coefficient of the signals after propagating through l layers in a ReLU network. We calculate the length and the correlation coefficient for $M = 1024$ input signals, averaged over 40 networks with a constant width $N = 2048$. In the first panel, the dashed line indicates the theoretical phase boundary $\sigma_w^2 = 2$ and the solid black line denotes the theoretical prediction for the length's fixed point. Note that the apparent crossing point before $\sigma_w^2 = 2$ is a finite size artifact and the phase boundary is indeed at $\sigma_w^2 = 2$. As the critical boundaries do not depend on the variance of bias, we show results for $\sigma_b^2 = 0.1$ only.

As correlations between two signals always converge to one, ReLU networks may not be very expressive. Multiple studies suggest that ReLU networks are biased towards simpler functions, supporting the observation. If that is the case, then ReLU networks should be incapable of performing complex tasks. However, they do work in practice, despite their poor expressive power. Of particular interest are two studies, which suggest that ReLU networks can be more expressive with anti-correlated weights. Ref. [49] found that a trained ReLU CNN's feature matrices are negatively correlated. Another study, Ref. [41], reveals that ReLU networks with anti-correlated weights explore a richer function space on applying perturbations when compared with those with uncorrelated weights. This motivated us to analyze the critical properties of anti-correlated ReLU networks.

3 Mean field analysis of signal propagation with correlated weights

In this section, we provide a mean-field analysis complementary to that of ReLU networks with anti-correlated weights. Unlike Ref. [41, 42], which studies perturbation around a ReLU network, our analysis aims to understand the critical properties of correlations. We consider correlations within the set of weights (\mathbf{w}_i^l) incoming to each neuron i , with all neurons identically distributed. The correlated Gaussian distribution is

$$P(\mathbf{w}_1^l, \mathbf{w}_2^l, \mathbf{w}_3^l \dots) = \prod_i \frac{\exp(-\frac{1}{2}(\mathbf{w}_i^l)^T A^{-1} \mathbf{w}_i^l)}{\sqrt{(2\pi)^{N_{l-1}} |A|}}, \quad (2)$$

with a covariance matrix given by

$$A = \frac{\sigma_w^2}{N_{l-1}} \left(\mathbb{I} - \frac{k}{1+k} \frac{J}{N_{l-1}} \right),$$

where \mathbb{I} is the identity matrix, J is an all-ones matrix, and k parameterizes the correlation strength. Positively correlated and anti-correlated regimes correspond to the regions $-1 < k < 0$ and $k > 0$, respectively. Note that weights reaching two different nodes are uncorrelated, and also the bias is uncorrelated with the weights.

We follow the same approach discussed in Section 2 to derive the length and correlation maps for ReLU networks with correlated weights given by Eqn. 2 (for derivation, see Appendix A.1). The length map turns out to be

$$q_h^l(x) = \frac{\sigma_w^2 q_h^{l-1}(x)}{2} \left(1 - \frac{k}{1+k} \frac{1}{\pi} \right) + \sigma_b^2.$$

The length is bounded if $\sigma_w^2 < 2 / \left(1 - \frac{k}{1+k} \frac{1}{\pi} \right)$. Thus, the boundary separating the ‘bounded’ and ‘unbounded’ phase shifts depending on the correlation strength. The boundary moves downward from that in the $k = 0$ case (see Fig. 1a) when the weights are positively correlated. In contrast, the boundary shifts upwards for anti-correlated weights.

We derive the covariance map similarly (for derivation, see Appendix A.2), which turns out to be

$$q_h^l(x_1, x_2) = \mathcal{C} \left(c_h^{l-1}(x_1, x_2), q_h^{l-1}(x_1), q_h^{l-1}(x_2) \right) - \frac{\sigma_w^2}{2} \frac{k}{k+1} \frac{1}{\pi} \sqrt{q_h^{l-1}(x_1) q_h^{l-1}(x_2)}.$$

By dividing the covariance by $q_h^*(x)$, we obtain the recursive map for the correlation coefficient

$$c_h^l(x_1, x_2) = \mathcal{C} \left(c_h^{l-1}(x_1, x_2), q_h^{l-1}(x_1), q_h^{l-1}(x_2) \right) / q_h^*(x) - \frac{\sigma_w^2}{2} \frac{k}{k+1} \frac{1}{\pi},$$

where the covariance map \mathcal{C} is the same as in Eqn. 1. It is easy to see that $c^*(x_1, x_2) = 1$ is always a fixed point. Next, we determine the stability of the fixed point $c_{12}^*(x_1, x_2) = 1$ by calculating $\frac{\partial c_{12}^l}{\partial c_{12}^{l-1}}$ evaluated at the fixed point. The fixed point’s stability depends only on the covariance map \mathcal{C} , and is given by

$$\chi_1 = \frac{\partial c_h^l(x_1, x_2)}{\partial c_h^{l-1}(x_1, x_2)} \Big|_{c_h^{l-1}(x_1, x_2)=1} = \sigma_w^2 \int Dz [\phi'(\sqrt{q^*(x)} z)]^2 = \frac{\sigma_w^2}{2}.$$

Equating the above equation to one, we obtain the phase transition boundary to be at $\sigma_w^2 = 2$. Note that the condition for the phase transition turns out to be the same for ReLU networks with uncorrelated weights. However, for uncorrelated weights, the condition is invalid as $q_h^l(x)$ diverges for $\sigma_w^2 \geq 2$.

In summary, the fixed point boundary for the length shifts depending on the correlation type, whereas the fixed point boundary for the correlation coefficient remains the same. For the positively correlated weights, the length’s fixed point boundary shifts downwards, resulting in similar phase space as for uncorrelated weights. In contrast, an interesting situation occurs for the anti-correlated weights. The fixed point boundary for the length shifts upwards, creating an opportunity for a ‘chaotic’ phase (see Fig. 1b). Such a ReLU network has three phases. First, an ordered bounded phase, where the length has a finite fixed point and correlations converge to one. Second an ordered ‘chaotic’ phase where the length still reaches a finite fixed point, but the correlations do not converge to one. Lastly, an unbounded chaotic phase, where the length of the signal diverges. We demonstrate these results numerically in Fig. 3 for a correlation strength of $k = 100$. As predicted by the above equations, the stability of the fixed point $c_{12}^*(x_1, x_2) = 1$ changes at $\sigma_w^2 = 2$, and the length diverges for a higher value of σ_w^2 .

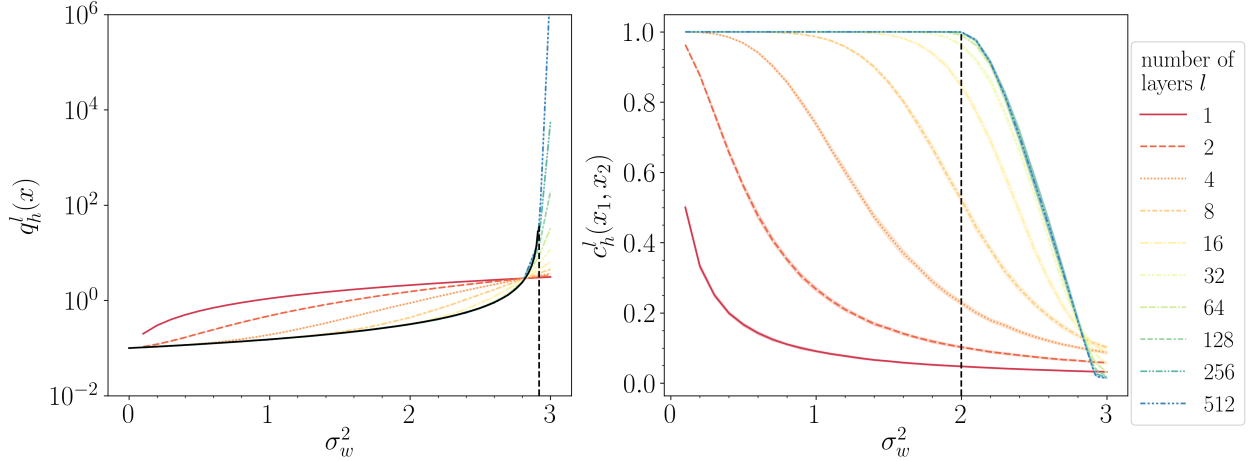


Figure 3: The above plots show the length and correlation coefficient of the signals after it has propagated through l layers in a ReLU network with anti-correlated weights. We calculate the length and the correlation coefficient for $M = 1024$ input signals, averaged over 40 networks with $N = 2048$ neurons in each layer. The dashed lines indicate the theoretical phase boundaries at $\sigma_w^2 = 2.92$ and $\sigma_w^2 = 2.0$ for the length and correlation coefficient. The solid black line in the first panel denotes the theoretical prediction for the length’s fixed point. As in Fig. 1a, the apparent crossing point before $\sigma_w^2 = 2.92$ is a finite size artifact. As the critical boundaries do not depend on the variance of bias, we show results just for $\sigma_b^2 = 0.1$.

In conclusion, a ReLU network with anti-correlated weights can be more expressive by taking advantage of a chaotic phase, and it may be beneficial for a ReLU network to remain in this subspace. Thus, we propose initializing ReLU networks with anti-correlated weights at the phase transition boundary of the correlation coefficient $(\sigma_w^2, \sigma_b^2) = (2, 0)$. We call it Anti-Correlated Initialization (ACI). Section 5 shows numerical results for the dynamics and performance of ReLU networks initialized with ACI for various tasks described in the next section.

4 Training tasks

This section describes various tasks used to analyze the dynamics and performance of different initialization schemes. We consider a variant of teacher-student setup [51], in which a student network is trained with examples generated by an untrained teacher network. We consider an $L = 10$ layered student neural network with $N = 100$ neurons in each layer trained using SGD and Adam algorithms. We consider three different tasks with varying complexities.

1. A standard teacher task, in which the training data is generated by a ReLU network of the same size as the student network, initialized using He initialization.
2. Next, we consider a simple teacher task, in which the capacity of the teacher task is much lower than the student network. In many real data sets, the high-dimensional inputs lie in a low-dimensional manifold [52], which motivates us to consider an easy teacher task. We consider a single-layer ReLU network with only $N = 10$ neurons, initialized with He initialization.
3. Lastly, we consider a complex teacher task, in which the complexity of the teacher network is more than the student network. We consider a teacher network with tanh activation of the same size as the student initialized in the chaotic regime [36], $(\sigma_w^2, \sigma_b^2) = (1.5, 0)$ (For ReLU

networks initialized with symmetric distributions, half of the neurons are dead. Thus, the effective capacity of a ReLU network is half its size).

The various tasks are summarized in Table 1. We implement neural networks in Tensorflow (version 2.2.0) [53] and train them with a mean squared error loss with a mini-batch size of 1000 and default parameters for the optimizers.

Task	size of teacher network	activation	(σ_w^2, σ_b^2)
standard task	same as student network	ReLU	(2, 0)
simple task	single hidden layer with 10 neurons	ReLU	(2, 0)
complex task	same as student network	tanh	(1.5, 0)

Table 1: Three tasks used to probe the dynamics and performance of different initialization schemes.

5 Training with Anti-Correlated Initialization

This section shows the dynamics and performance of ReLU networks initialized with different weight correlation strength k on tasks described in Section 4. We choose three different correlation strengths; $k = 100$ induces anti-correlated weights, $k = -0.5$ produces positively correlated weights, and lastly, $k = 0$ corresponds to uncorrelated weights (He initialization). We train networks with two different optimization algorithms, SGD and Adam. For SGD, we train for 10^4 epochs, and for Adam, we train for 10^3 epochs.

5.1 Standard teacher task

Fig. 4a and 4b show the average validation loss for different correlation strengths trained using SGD and Adam algorithms. We observe that ReLU networks initialized with ACI ($k = 100$) train faster than He initialization ($k = 0$). In contrast, ReLU networks with positively correlated weights ($k = -0.5$) train even slower than He initialization.

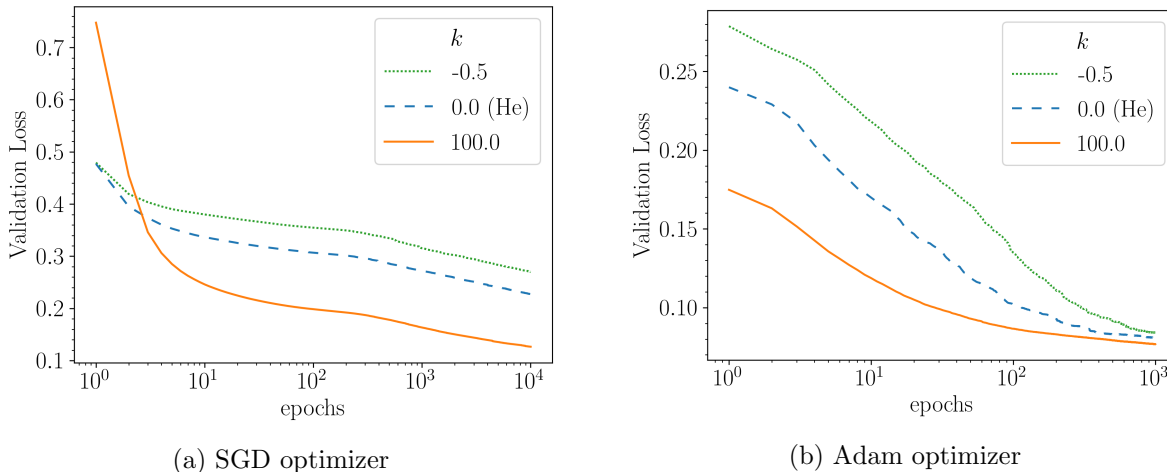


Figure 4: Average validation loss of 100 ReLU networks trained on the standard teacher task for different weight correlation strengths.

5.2 Simple teacher task

Fig. 5a and 5b show the average validation loss for the simple teacher task. We observe similar qualitative results as in the standard teacher task. For SGD, we observe an initial linear region in which all initialization schemes perform equally.

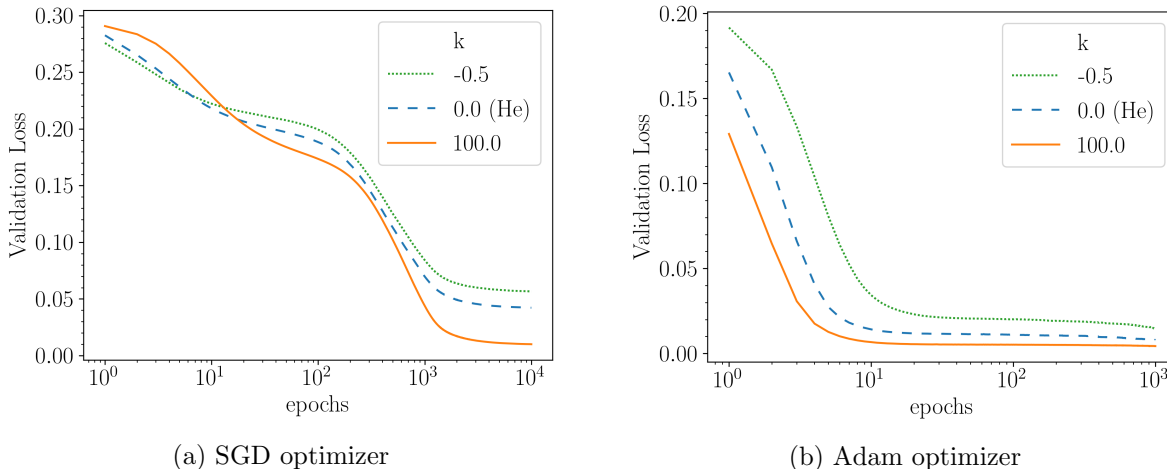


Figure 5: Average validation loss of 100 ReLU networks trained on the simple teacher task for different weight correlation strengths.

5.3 Complex teacher task

Fig. 6a and 6b show the average validation loss for a complex teacher task. For some intermediate regions, ACI performs worse than other initializations on training with SGD. The regions where ACI performs poorly shift depending on the complexity of the task.

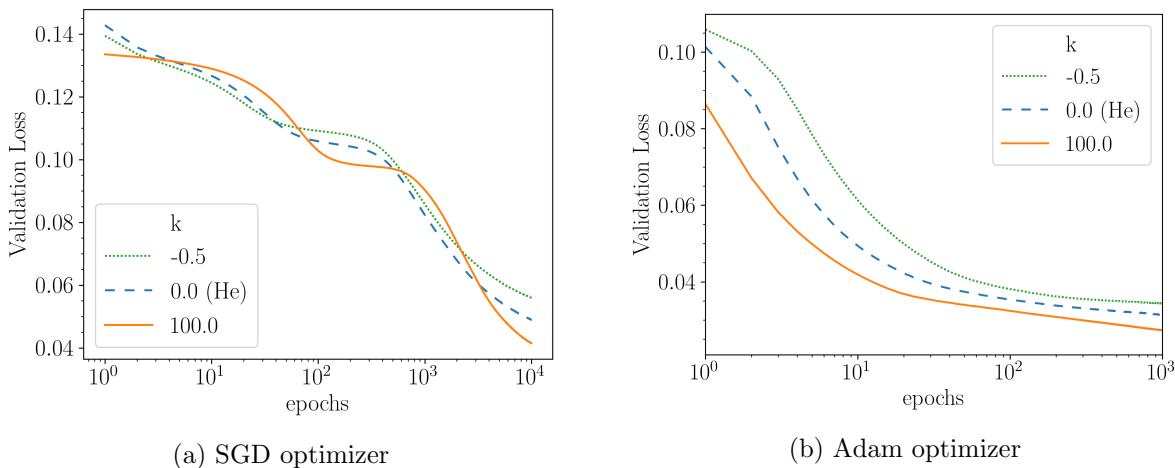


Figure 6: Average validation loss for ReLU networks trained on the complex teacher task for different weight correlation strengths.

Many alternatives are proposed to improve ReLU networks by reducing the dead node probability [16, 18, 19]. Of particular interest is Random Asymmetric Initialization (RAI), which replaces

one of the weight/biases incoming to a neuron with a random variable drawn from a beta distribution to reduce the dead node probability. In the next section, we first analyze the correlation properties of RAI and then combine it with ACI to propose a new initialization scheme RAAI, which performs better than the best-known initialization schemes for ReLU networks.

6 Random Asymmetric Anti-correlated Initialization

We begin by analyzing critical properties of Random Asymmetric Initialization (RAI) proposed by Ref. [18] to reduce dead node probability. For ReLU networks with symmetric distributions for weights and biases, the probability of a dead node is half, and RAI reduces it by initializing one of the weights/bias incoming to neuron by a distribution with positive support (like the beta distribution), resulting in a positive mean for the pre-activations. Ref. [18] propose to initialize RAI with a variance $\sigma_w^2 = 0.36$ to ensure that the signal’s length is bounded. We analyzed the correlation properties of RAI and found that $c_h^l(x_1, x_2) = 1$ is always a fixed point of the dynamics (see Appendix B.2). Finding the stability of the fixed point $c_h^*(x_1, x_2) = 1$ even with the mean-field assumptions is difficult. In Appendix C.2, we estimate the fixed point boundary for the length and correlation coefficient approximately. We found that the length has a finite non-zero fixed point if $\sigma_w^2 < 0.56$. In Fig. 7, we show the numerical results for the fixed points of length and correlation coefficient. This suggests that the length remains finite for σ_w^2 up to 0.72 (first panel), and the $c_h^*(x_1, x_2) = 1$ is always a stable fixed point of the dynamics (second panel). The approximated results thus underestimate the length’s critical point.

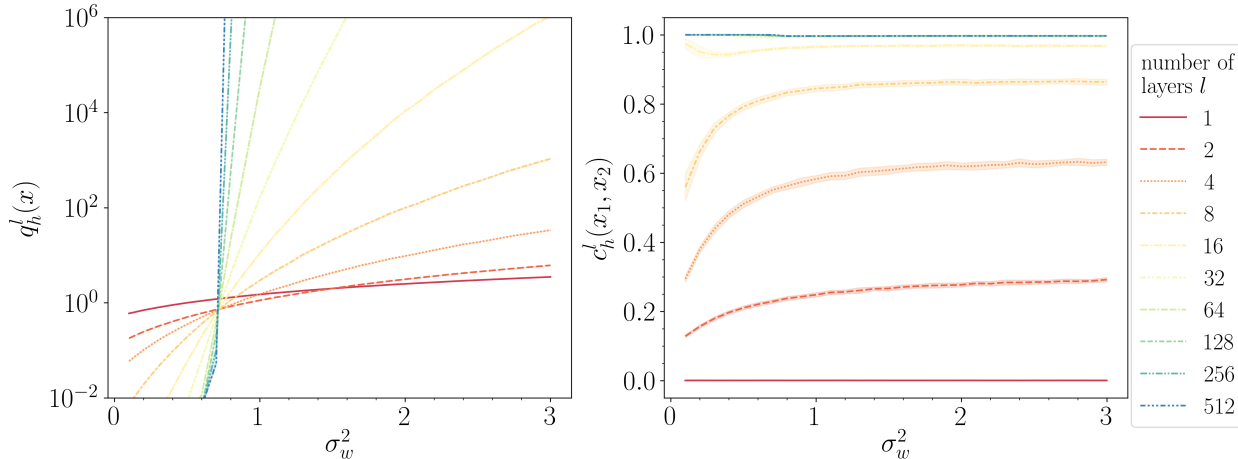


Figure 7: The above plots show the length and the correlation coefficient of the signals after propagating through l layers in a ReLU network initialized with RAI. We calculate the length and the correlation coefficient for $M = 1024$ input signals, averaged over 40 networks with $N = 2048$ neurons in each layer.

RAI focuses on decreasing the dead node probability to increase expressive power, whereas ACI uses anti-correlated weights to improve the expressivity. As RAI and ACI increase the expressivity of a ReLU network using different mechanisms, we explore the possibility of combining the two. We call it Random Anti-correlated Asymmetric Initialization (RAAI). To prepare weights drawn from RAAI, we take anti-correlated weights and biases incoming to a neuron (like Eqn. 2) and replace a randomly picked weight/bias with a random variable drawn from a beta distribution. Note that the weights incoming to different neurons are uncorrelated. Like ACI, we expect three

phases, and we do observe the same in an approximate analysis of RAAI (see Appendix D). We find that the length diverges when $\sigma_w^2 > 1.75$, whereas the fixed point $c^*(x_1, x_2) = 1$ becomes unstable at $\sigma_w^2 = 1.41$. This again opens a possibility for a chaotic phase. We numerically verify these results in Fig. 8. We find that the length diverges for $\sigma_w^2 > 1.2$, whereas the correlation’s fixed point is around $\sigma_w^2 = 0.9$. The numerical results qualitatively agree with our analysis, although the approximation in the analysis leads to overestimation of the phase boundaries.

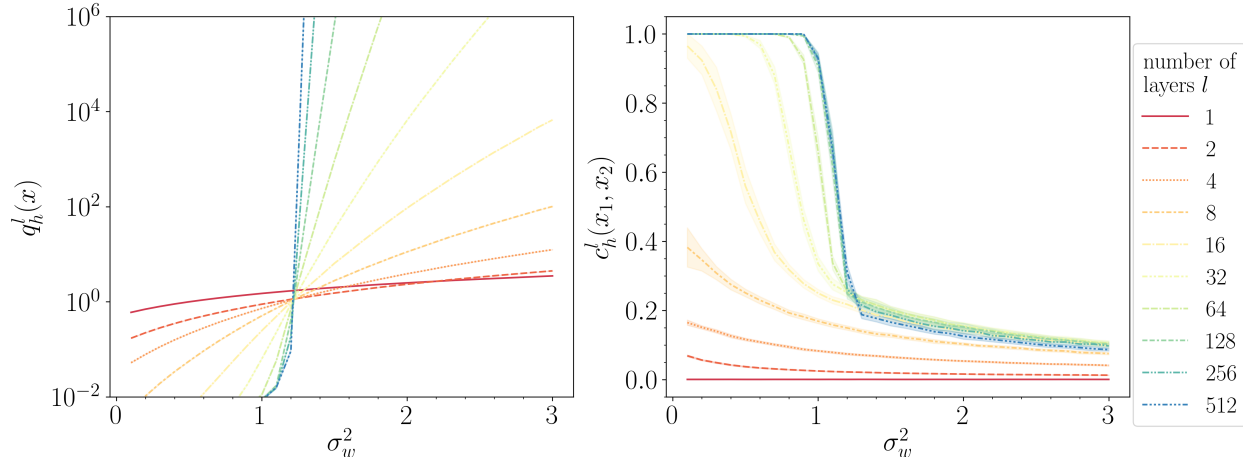


Figure 8: The above plots show length and the correlation coefficient of the signals after it has propagated through l layers in a ReLU network initialized with RAAI. We calculate the length and the correlation coefficient for $M = 1024$ input signals, averaged over 40 networks with $N = 2048$ neurons in each layer.

In summary, RAAI, unlike RAI, also has a chaotic phase, and it has a lower dead node probability too. Thus, we expect RAAI to be a strong candidate for initializing ReLU networks. In Table 2, we summarize and compare different initialization schemes. The dead node probabilities are calculated numerically for input signals drawn from the standard normal distribution.

Initialization scheme	σ_w^2	k	Chaotic phase	Dead node probability
He	2.0	0.0	No	0.5
ACI	2.0	100.0	Yes	0.5
RAI	0.36	0.0	No	0.36
RAAI	0.92	100.0	Yes	0.36

Table 2: Comparison between different initialization schemes for ReLU networks. RAI and RAAI both have a lower dead node probability than the other two symmetric initializations. ACI and RAAI have a chaotic phase, whereas the other two do not. Thus, RAAI has both a chaotic phase and a lower dead node probability.

In the next section, we analyze the dynamics and performance of RAAI and compare it with other initialization schemes.

7 Training with RAAI

This section compares the performance of RAAI with other initialization schemes listed in Table 2 on tasks described in Section 4.

7.1 Standard teacher task

Fig. 9a and 9b show the average validation loss for different initialization schemes described in Table 2 trained using SGD and Adam algorithms. We observe that RAAI performs on par with or better than all other initialization schemes, whereas the relative performance of RAI and ACI depends on the optimization algorithm.

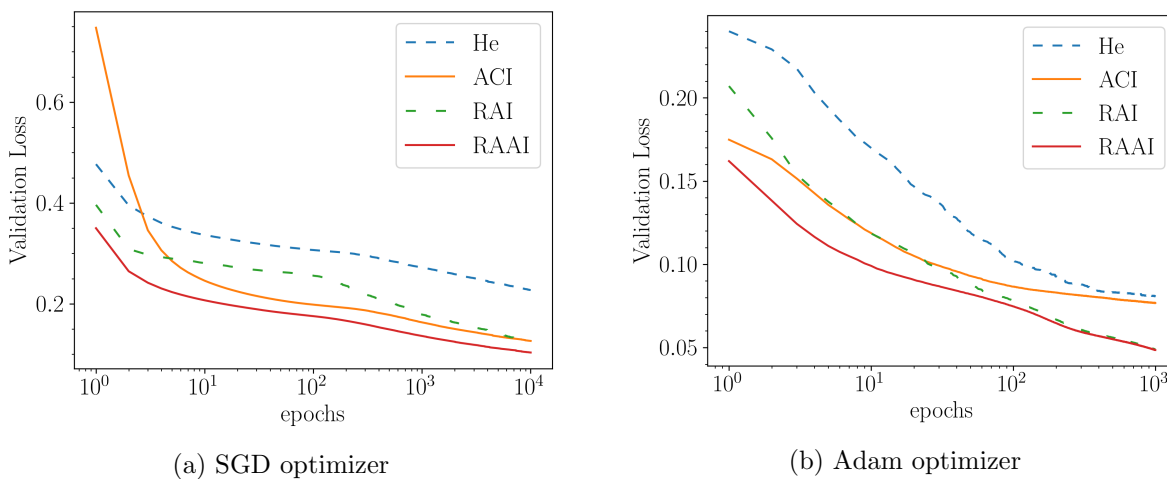


Figure 9: Average validation loss for ReLU networks trained on the standard teacher task for different initialization schemes.

7.2 Simple teacher task

Fig. 10a and 10b show the average validation loss for the simple teacher task for different initialization schemes. Similar to the standard teacher task, RAAI performs better than or on par with other initialization schemes. In between RAI and ACI, the former performs better on using either optimizers.

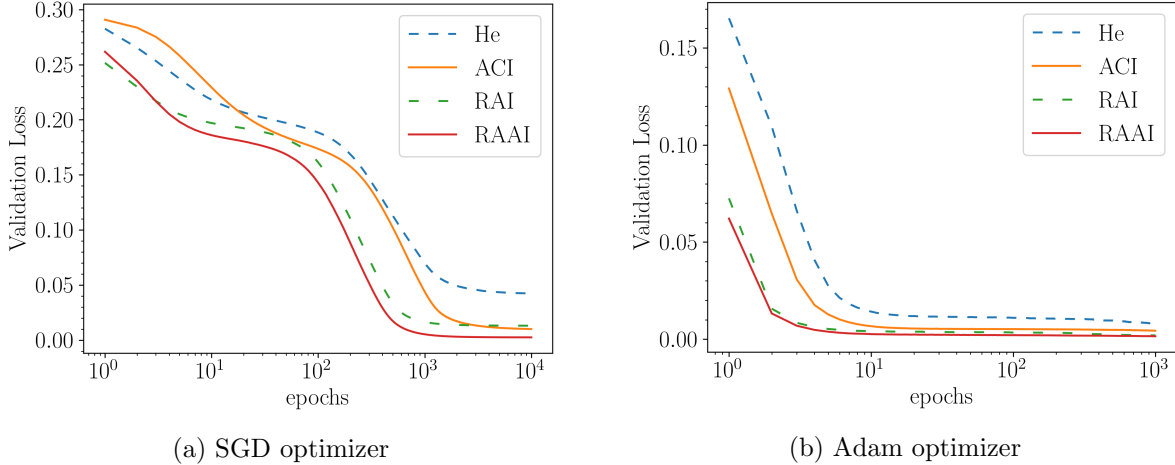


Figure 10: Average validation loss for ReLU networks trained on the simple teacher task for different initialization schemes.

7.3 Complex teacher task

Fig. 7 and 8 show the average validation loss for a complex teacher task. Again, RAAI performs better than or on par with all other initialization schemes.

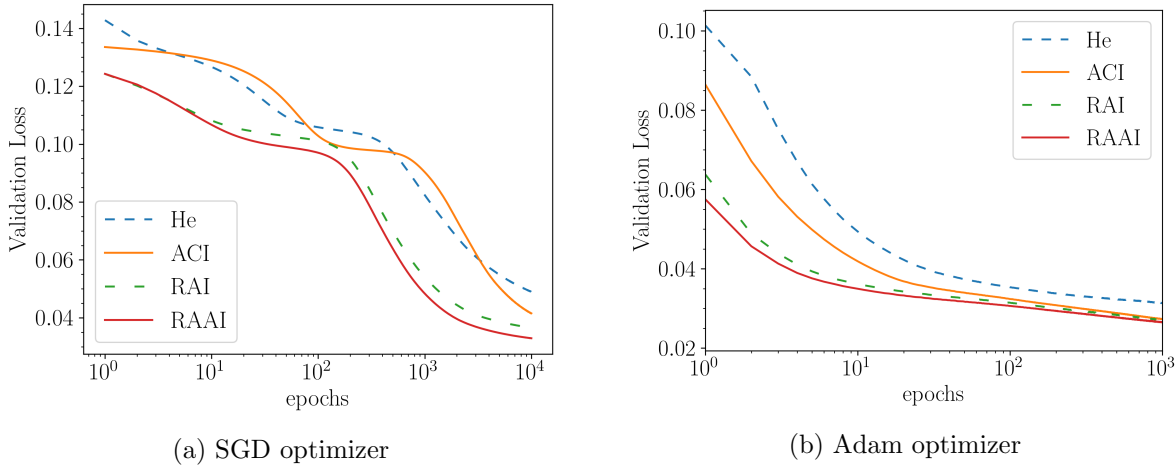


Figure 11: Average validation loss for ReLU networks trained on the complex teacher task for different initialization schemes.

It may be of concern that initialization in an expressive subspace of weights might lead to overfitting. We trained a neural network with $L = 20$ layers and found that ACI starts to overfit, but this can be avoided by reducing the value of the correlation strength k . This leads to another parameter to be tuned. On the other hand, RAAI does not show any overfitting signs and performs consistently better than other initialization schemes on training deeper networks. We believe that overfitting in ACI is related to correlations vanishing to zero at high variance (see Fig. 3). In contrast, for RAAI, correlations do not vanish to zero at high variance (see Fig. 8).

8 Discussion and Conclusion

In this article, we analyzed the evolution of correlation between signals propagating through a ReLU network with correlated weights using the mean-field theory of signal propagation. Multiple studies show that ReLU networks with uncorrelated weights are biased towards computing simpler functions, but ReLU networks do perform complex tasks in practice. Unlike ReLU networks with uncorrelated weights, ReLU networks with anti-correlated weights reaching a node have a chaotic phase where correlation saturates below unity. This suggests that such networks can exhibit higher expressivity. Although we have focused on the ReLU networks in this study, anti-correlation in weights may be useful in general. Networks with other non-linear activation functions like tanh, SELU, and sigmoid have a chaotic phase even with uncorrelated weights. In these cases, the weight correlations may still help to tune the phase boundaries and expressivity of the networks.

We further investigated the possibility that ReLU networks with the enhanced expressivity may prove beneficial in faster learning. Comparison of training and test performance of networks in a range of teacher-student setups clearly showed that networks with anti-correlated weights learn faster. While ACI shows better learning performance in general, it shows poor performance with SGD during an intermediate learning stage when the teacher network has a relatively higher capacity. We believe that this may be due to the system getting stuck in local minima. This is consistent with the absence of a similar regime on training with Adam optimizer. On training deeper networks with ACI, we found that it overfits, but this can be avoided by fine-tuning correlation strength k . We also investigated improvement in training time from a regularization term in the loss function that favors anti-correlated weights, but our attempts did not show any systematic results.

We compared ACI with a recently proposed initialization scheme called RAI, which introduces a systematic asymmetry (around 0) in the weights to decrease dead ReLU probability. We find that the relative performance between RAI and ACI depends on the task and the optimization algorithm. RAI improves expressivity by reducing the dead node probability, whereas ACI achieves the same by inducing a chaotic phase. As RAI and ACI rely on different mechanisms, we explored a strategy of combining the two initialization schemes. We analyzed the correlation properties of RAAI and found that it has a chaotic phase like ACI. We demonstrated that RAAI leads to faster training and learning than the best-known methods on various teacher tasks of a range of complexity. For different initialization schemes, the behavior of the training dynamics at large epochs may depend on the optimizer and training data, however RAAI shows a definite advantage over other schemes when using the SGD optimizer, especially in early training epochs. In addition to faster training, RAAI also shows no sign of overfitting and thus improves on the simpler strategy that relies only on anticorrelations.

Acknowledgments

Dayal Singh would like to acknowledge the INSPIRE-SHE programme of Department of Science & Technology, India. G J Sreejith acknowledges National Supercomputing Mission (Param Bramha, IISER Pune) for computational resources and financial support.

References

- [1] K. Fukushima. Visual feature extraction by a multilayered network of analog threshold elements. *IEEE Transactions on Systems Science and Cybernetics*, 5(4):322–333, 1969.

- [2] Kuniyiko Fukushima and Sei Miyake. Neocognitron: A self-organizing neural network model for a mechanism of visual pattern recognition. In Shun-ichi Amari and Michael A. Arbib, editors, *Competition and Cooperation in Neural Nets*, pages 267–285, Berlin, Heidelberg, 1982. Springer Berlin Heidelberg.
- [3] Yann LeCun, Y. Bengio, and Geoffrey Hinton. Deep learning. *Nature*, 521:436–44, 05 2015.
- [4] Prajit Ramachandran, Barret Zoph, and Quoc V. Le. Searching for activation functions, 2018.
- [5] Vinod Nair and Geoffrey E. Hinton. Rectified linear units improve restricted boltzmann machines. In *Proceedings of the 27th International Conference on International Conference on Machine Learning*, ICML’10, page 807–814, Madison, WI, USA, 2010. Omnipress.
- [6] Xavier Glorot, Antoine Bordes, and Yoshua Bengio. Deep sparse rectifier neural networks. In Geoffrey Gordon, David Dunson, and Miroslav Dudík, editors, *Proceedings of the Fourteenth International Conference on Artificial Intelligence and Statistics*, volume 15 of *Proceedings of Machine Learning Research*, pages 315–323, Fort Lauderdale, FL, USA, 11–13 Apr 2011. JMLR Workshop and Conference Proceedings.
- [7] Alex Krizhevsky, Ilya Sutskever, and Geoffrey E Hinton. Imagenet classification with deep convolutional neural networks. In F. Pereira, C. J. C. Burges, L. Bottou, and K. Q. Weinberger, editors, *Advances in Neural Information Processing Systems*, volume 25, pages 1097–1105. Curran Associates, Inc., 2012.
- [8] Kaiming He, Xiangyu Zhang, Shaoqing Ren, and Jian Sun. Delving deep into rectifiers: Surpassing human-level performance on imagenet classification. *IEEE International Conference on Computer Vision (ICCV 2015)*, 1502, 02 2015.
- [9] Andrew L. Maas, Awni Y. Hannun, and Andrew Y. Ng. Rectifier nonlinearities improve neural network acoustic models. In *in ICML Workshop on Deep Learning for Audio, Speech and Language Processing*, 2013.
- [10] L. Tóth. Phone recognition with deep sparse rectifier neural networks. *2013 IEEE International Conference on Acoustics, Speech and Signal Processing*, pages 6985–6989, 2013.
- [11] G. Hinton, L. Deng, D. Yu, G. E. Dahl, A. Mohamed, N. Jaitly, A. Senior, V. Vanhoucke, P. Nguyen, T. N. Sainath, and B. Kingsbury. Deep neural networks for acoustic modeling in speech recognition: The shared views of four research groups. *IEEE Signal Processing Magazine*, 29(6):82–97, 2012.
- [12] David Silver, Aja Huang, Christopher Maddison, Arthur Guez, Laurent Sifre, George Driessche, Julian Schrittwieser, Ioannis Antonoglou, Veda Panneershelvam, Marc Lanctot, Sander Dieleman, Dominik Grewe, John Nham, Nal Kalchbrenner, Ilya Sutskever, Timothy Lillicrap, Madeleine Leach, Koray Kavukcuoglu, Thore Graepel, and Demis Hassabis. Mastering the game of go with deep neural networks and tree search. *Nature*, 529:484–489, 01 2016.
- [13] Alireza Seif, M. Hafezi, and C. Jarzynski. Machine learning the thermodynamic arrow of time. *Nature Physics*, 17:105–113, 2019.
- [14] Xavier Glorot, Antoine Bordes, and Yoshua Bengio. Deep sparse rectifier neural networks. In Geoffrey Gordon, David Dunson, and Miroslav Dudík, editors, *Proceedings of the Fourteenth International Conference on Artificial Intelligence and Statistics*, volume 15 of *Proceedings*

- of Machine Learning Research*, pages 315–323, Fort Lauderdale, FL, USA, 11–13 Apr 2011. JMLR Workshop and Conference Proceedings.
- [15] Hartmut Maennel, O. Bousquet, and S. Gelly. Gradient descent quantizes relu network features. *ArXiv*, abs/1803.08367, 2018.
 - [16] Ludovic Trottier, P. Giguère, and B. Chaib-draa. Parametric exponential linear unit for deep convolutional neural networks. *2017 16th IEEE International Conference on Machine Learning and Applications (ICMLA)*, pages 207–214, 2017.
 - [17] Boris Hanin. Which neural net architectures give rise to exploding and vanishing gradients? In S. Bengio, H. Wallach, H. Larochelle, K. Grauman, N. Cesa-Bianchi, and R. Garnett, editors, *Advances in Neural Information Processing Systems*, volume 31, pages 582–591. Curran Associates, Inc., 2018.
 - [18] Lu Lu, Yeonjong Shin, Yanhui Su, and George Karniadakis. Dying relu and initialization: Theory and numerical examples. *Communications in Computational Physics*, 28:1671–1706, 11 2020.
 - [19] Djork-Arné Clevert, Thomas Unterthiner, and Sepp Hochreiter. Fast and accurate deep network learning by exponential linear units (elus). In Yoshua Bengio and Yann LeCun, editors, *4th International Conference on Learning Representations, ICLR 2016, San Juan, Puerto Rico, May 2-4, 2016, Conference Track Proceedings*, 2016.
 - [20] Günter Klambauer, Thomas Unterthiner, Andreas Mayr, and Sepp Hochreiter. Self-normalizing neural networks. In I. Guyon, U. V. Luxburg, S. Bengio, H. Wallach, R. Fergus, S. Vishwanathan, and R. Garnett, editors, *Advances in Neural Information Processing Systems*, volume 30, pages 971–980. Curran Associates, Inc., 2017.
 - [21] Dan Hendrycks and Kevin Gimpel. Gaussian error linear units (gelus). *arXiv: Learning*, 2016.
 - [22] Kaiming He, X. Zhang, Shaoqing Ren, and Jian Sun. Deep residual learning for image recognition. *2016 IEEE Conference on Computer Vision and Pattern Recognition (CVPR)*, pages 770–778, 2016.
 - [23] Lei Jimmy Ba, Jamie Ryan Kiros, and Geoffrey E. Hinton. Layer normalization. *CoRR*, abs/1607.06450, 2016.
 - [24] Sergey Ioffe and Christian Szegedy. Batch normalization: Accelerating deep network training by reducing internal covariate shift. In Francis Bach and David Blei, editors, *Proceedings of the 32nd International Conference on Machine Learning*, volume 37 of *Proceedings of Machine Learning Research*, pages 448–456, Lille, France, 07–09 Jul 2015. PMLR.
 - [25] Tim Salimans and Diederik P. Kingma. Weight normalization: A simple reparameterization to accelerate training of deep neural networks. In *NIPS*, 2016.
 - [26] D. Ulyanov, A. Vedaldi, and V. Lempitsky. Instance normalization: The missing ingredient for fast stylization. *ArXiv*, abs/1607.08022, 2016.
 - [27] Yuxin Wu and Kaiming He. Group normalization. In *ECCV*, 2018.
 - [28] Dmytro Mishkin and Jiri Matas. All you need is a good init. *CoRR*, abs/1511.06422, 2016.

- [29] Diederik P. Kingma and Jimmy Ba. Adam: A method for stochastic optimization. *CoRR*, abs/1412.6980, 2015.
- [30] Matthew D. Zeiler. Adadelta: An adaptive learning rate method. *ArXiv*, abs/1212.5701, 2012.
- [31] John C. Duchi, Elad Hazan, and Y. Singer. Adaptive subgradient methods for online learning and stochastic optimization. In *J. Mach. Learn. Res.*, 2011.
- [32] Simon Du, Jason Lee, Haochuan Li, Liwei Wang, and Xiyu Zhai. Gradient descent finds global minima of deep neural networks. In Kamalika Chaudhuri and Ruslan Salakhutdinov, editors, *Proceedings of the 36th International Conference on Machine Learning*, volume 97 of *Proceedings of Machine Learning Research*, pages 1675–1685. PMLR, 09–15 Jun 2019.
- [33] Rupesh Srivastava, Klaus Greff, and Jürgen Schmidhuber. Training very deep networks. *2015 Neural Information Processing Systems (NIPS 2015 Spotlight)*, 07 2015.
- [34] Yurii Nesterov. *Introductory Lectures on Convex Optimization: A Basic Course*. Springer Publishing Company, Incorporated, 1 edition, 2014.
- [35] Andrew M. Saxe, James L. McClelland, and Surya Ganguli. Exact solutions to the nonlinear dynamics of learning in deep linear neural networks. In Yoshua Bengio and Yann LeCun, editors, *2nd International Conference on Learning Representations, ICLR 2014, Banff, AB, Canada, April 14-16, 2014, Conference Track Proceedings*, 2014.
- [36] Ben Poole, Subhaneil Lahiri, Maithra Raghu, Jascha Sohl-Dickstein, and Surya Ganguli. Exponential expressivity in deep neural networks through transient chaos. In D. Lee, M. Sugiyama, U. Luxburg, I. Guyon, and R. Garnett, editors, *Advances in Neural Information Processing Systems*, volume 29, pages 3360–3368. Curran Associates, Inc., 2016.
- [37] Maithra Raghu, Ben Poole, Jon Kleinberg, Surya Ganguli, and Jascha Sohl-Dickstein. On the expressive power of deep neural networks. In *Proceedings of the 34th International Conference on Machine Learning - Volume 70*, ICML’17, page 2847–2854. JMLR.org, 2017.
- [38] Samuel S. Schoenholz, Justin Gilmer, Surya Ganguli, and Jascha Sohl-Dickstein. Deep information propagation. In *5th International Conference on Learning Representations, ICLR 2017, Toulon, France, April 24-26, 2017, Conference Track Proceedings*. OpenReview.net, 2017.
- [39] Jaehoon Lee, Jascha Sohl-dickstein, Jeffrey Pennington, Roman Novak, Sam Schoenholz, and Yasaman Bahri. Deep neural networks as gaussian processes. In *International Conference on Learning Representations*, 2018.
- [40] Soufiane Hayou, Arnaud Doucet, and Judith Rousseau. On the selection of initialization and activation function for deep neural networks, 2019.
- [41] Bo Li and David Saad. Exploring the function space of deep-learning machines. *Phys. Rev. Lett.*, 120:248301, Jun 2018.
- [42] Bo Li and David Saad. Large deviation analysis of function sensitivity in random deep neural networks. *Journal of Physics A: Mathematical and Theoretical*, 53(10):104002, feb 2020.
- [43] Yasaman Bahri, Jonathan Kadmon, Jeffrey Pennington, Sam S. Schoenholz, Jascha Sohl-Dickstein, and Surya Ganguli. Statistical mechanics of deep learning. *Annual Review of Condensed Matter Physics*, 11(1):501–528, 2020.

- [44] Giacomo De Palma, Bobak Kiani, and Seth Lloyd. Random deep neural networks are biased towards simple functions. In H. Wallach, H. Larochelle, A. Beygelzimer, F. d'Alché-Buc, E. Fox, and R. Garnett, editors, *Advances in Neural Information Processing Systems*, volume 32, pages 1964–1976. Curran Associates, Inc., 2019.
- [45] Nasim Rahaman, Aristide Baratin, Devansh Arpit, Felix Draxler, Min Lin, Fred Hamprecht, Yoshua Bengio, and Aaron Courville. On the spectral bias of neural networks, 2019.
- [46] Juncai He, Lin Li, Jinchao Xu, and Chunyue Zheng. Relu deep neural networks and linear finite elements. *Journal of Computational Mathematics*, 38(3):502–527, 2020.
- [47] Guillermo Valle-Perez, Chico Q. Camargo, and Ard A. Louis. Deep learning generalizes because the parameter-function map is biased towards simple functions. In *International Conference on Learning Representations*, 2019.
- [48] B. Hanin and D. Rolnick. Deep relu networks have surprisingly few activation patterns. In *NeurIPS*, 2019.
- [49] Wenling Shang, Kihyuk Sohn, Diogo Almeida, and Honglak Lee. Understanding and improving convolutional neural networks via concatenated rectified linear units. In *Proceedings of the 33rd International Conference on International Conference on Machine Learning - Volume 48*, ICML'16, page 2217–2225. JMLR.org, 2016.
- [50] Soufiane Hayou, Arnaud Doucet, and Judith Rousseau. On the impact of the activation function on deep neural networks training. In Kamalika Chaudhuri and Ruslan Salakhutdinov, editors, *Proceedings of the 36th International Conference on Machine Learning*, volume 97 of *Proceedings of Machine Learning Research*, pages 2672–2680. PMLR, 09–15 Jun 2019.
- [51] H. S. Seung, H. Sompolinsky, and N. Tishby. Statistical mechanics of learning from examples. *Phys. Rev. A*, 45:6056–6091, Apr 1992.
- [52] Sebastian Goldt, Marc Mezard, Florent Krzakala, and Lenka Zdeborova. Modeling the influence of data structure on learning in neural networks: The hidden manifold model. *Physical Review X*, 10, 12 2020.
- [53] Martín Abadi, Ashish Agarwal, Paul Barham, Eugene Brevdo, Zhifeng Chen, Craig Citro, Greg Corrado, Andy Davis, Jeffrey Dean, Matthieu Devin, Sanjay Ghemawat, Ian Goodfellow, Andrew Harp, Geoffrey Irving, Michael Isard, Yangqing Jia, Rafal Jozefowicz, Lukasz Kaiser, Manjunath Kudlur, Josh Levenberg, Dan Mané, Rajat Monga, Sherry Moore, Derek Murray, Chris Olah, Mike Schuster, Jonathon Shlens, Benoit Steiner, Ilya Sutskever, Kunal Talwar, Paul Tucker, Vincent Vanhoucke, Vijay Vasudevan, Fernanda Viégas, Oriol Vinyals, Pete Warden, Martin Wattenberg, Martin Wicke, Yuan Yu, and Xiaoqiang Zheng. Tensorflow: Large-scale machine learning on heterogeneous distributed systems, 2015.
- [54] C. Szegedy, Wei Liu, Yangqing Jia, P. Sermanet, S. Reed, D. Anguelov, D. Erhan, V. Vanhoucke, and A. Rabinovich. Going deeper with convolutions. In *2015 IEEE Conference on Computer Vision and Pattern Recognition (CVPR)*, pages 1–9, 2015.
- [55] Abien Fred Agarap. Deep learning using rectified linear units (relu). *ArXiv*, abs/1803.08375, 2018.

A Derivation of the length and correlation maps for correlated weights

This section derives the length and covariance maps for ReLU networks with correlated weights given by Eqn. 2. For simplicity, we consider $N_l = N$ in all layers, but the results hold for all N_l , as long as it is large.

A.1 Derivation of length map

To derive the length map, we follow the approach discussed in Section 2. Assuming self-averaging, we obtain the average value of the length of a signal, x , reaching layer l by considering an average over weights and biases as

$$\begin{aligned} q_h^l(x) &= \frac{1}{N} \left\langle \sum_{i=1}^N (h_i^l(x))^2 \right\rangle = \frac{1}{N} \sum_{i=1}^N \sum_{j,m=1}^N \langle w_{ij}^l w_{im}^l \rangle \phi(h_j^{l-1}(x)) \phi(h_m^{l-1}(x)) + \langle (b_i^l)^2 \rangle \\ &= \frac{\sigma_w^2}{N} \sum_{j,m=1}^N \left(\delta_{j,m} - \frac{k}{1+k} \frac{1}{N} \right) \phi(h_j^{l-1}(x)) \phi(h_m^{l-1}(x)) + \sigma_b^2, \end{aligned}$$

where we have used $\langle w_{ij}^l w_{im}^l \rangle = \delta_{j,m} - \frac{k}{1+k} \frac{1}{N}$ and $\langle (b_i^l)^2 \rangle = \sigma_b^2$. For large N , each $h_i^{l-1}(x)$ is a weighted sum of a large number of correlated random variables, which converges to a zero-mean Gaussian with a variance $q_h^{l-1}(x)$ (by the definition of $q_h^{l-1}(x)$). Replacing the average over all neurons at layer $l-1$ by a Gaussian distribution, we get

$$q_h^l(x) = \sigma_w^2 \int Dz \phi \left(\sqrt{q_h^{l-1}(x)} z \right)^2 - \sigma_w^2 \frac{k}{1+k} \left[\int Dz \phi \left(\sqrt{q_h^{l-1}(x)} z \right) \right]^2 + \sigma_b^2. \quad (3)$$

For the second term in Eqn. 3, we have used the fact that for $m \neq j$, $h_j^l(x)$ and $h_m^l(x)$ are uncorrelated random variables and ignored $\mathcal{O}(1/N)$ terms. Note that weights reaching two different nodes are uncorrelated. We can write Eqn. 3 in terms of the length map \mathcal{V} from Eqn. 1 to get

$$q_h^l(x) = \mathcal{V}(q_h^{l-1}(x) | \sigma_w^2, \sigma_b^2) - \sigma_w^2 \frac{k}{1+k} \left[\int Dz \phi \left(\sqrt{q_h^{l-1}(x)} z \right) \right]^2.$$

For a ReLU activation, we can perform the integrals to get the exact form of the recursive relation between $q_h^l(x)$ and $q_h^{l-1}(x)$ to be:

$$q_h^l(x) = \frac{\sigma_w^2 q_h^{l-1}(x)}{2} \left(1 - \frac{k}{1+k} \frac{1}{\pi} \right) + \sigma_b^2.$$

A.2 Derivation of the covariance map

The covariance map can be derived similarly by considering an average over the weights and biases

$$q_h^l(x_1, x_2) = \frac{1}{N} \left\langle \sum_{i=1}^N h_i^l(x_1) h_i^l(x_2) \right\rangle = \sum_{j,k=1}^N \langle w_{ij}^l w_{ik}^l \rangle \phi(h_j^{l-1}(x_1)) \phi(h_k^{l-1}(x_2)) + \langle (b_i^l)^2 \rangle$$

$$q_h^l(x_1, x_2) = \frac{\sigma_w^2}{N} \sum_{j,k=1}^N \left(\delta_{j,k} - \frac{k}{1+k} \frac{1}{N} \right) \phi(h_j^{l-1}(x_1)) \phi(h_k^{l-1}(x_2)) + \sigma_b^2,$$

and then replacing the sum over neurons in the previous layer with an integral with a Gaussian measure. For large N , the joint distribution of $h_j^l(x_1)$ and $h_k^l(x_2)$ will converge to a two-dimensional Gaussian distribution with a covariance $q_h^{l-1}(x_1, x_2)$. Propagating this joint distribution across one layer, we obtain the iterative map

$$q_h^l(x_1, x_2) = \sigma_w^2 \int Dz_1 Dz_2 \phi(u_1) \phi(u_2) - \sigma_w^2 \frac{k}{k+1} \int Dz_1 Dz_2 \phi(\sqrt{q_h^{l-1}(x_1)} z_1) \phi(\sqrt{q_h^{l-1}(x_2)} z_2) + \sigma_b^2$$

$$u_1 = \sqrt{q_h^{l-1}(x_1)} z_1, \quad u_2 = \sqrt{q_h^{l-1}(x_2)} \left[c_h^{l-1}(x_1, x_2) z_1 + \sqrt{1 - (c_h^{l-1}(x_1, x_2))^2} z_2 \right],$$
(4)

where $c_h^l(x_1, x_2) = q_h^l(x_1, x_2) / \sqrt{q_h^l(x_1) q_h^l(x_2)}$ is the correlation coefficient, and Dz_1, Dz_2 are standard normal Gaussian distributions. Again, in the second part of Eqn. 4, we have used the fact that for $k \neq j$, $h_j^l(x_1)$ and $h_k^l(x_2)$ are uncorrelated random variables and have ignored $\mathcal{O}(1/N)$ terms. We can further write Eqn. 4 in terms of the correlation map \mathcal{C} from Eqn. 1 to get

$$q_h^l(x_1, x_2) = \mathcal{C} \left(c_h^{l-1}(x_1, x_2), q_h^{l-1}(x_1), q_h^{l-1}(x_2) \mid \sigma_w^2, \sigma_b^2 \right)$$

$$- \sigma_w^2 \frac{k}{k+1} \int Dz_1 Dz_2 \phi(\sqrt{q_h^{l-1}(x_1)} z_1) \phi(\sqrt{q_h^{l-1}(x_2)} z_2)$$

Further, we can perform the integrals in the second part of the above equation to get

$$q_h^l(x_1, x_2) = \mathcal{C} \left(c_h^{l-1}(x_1, x_2), q_h^{l-1}(x_1), q_h^{l-1}(x_2) \mid \sigma_w^2, \sigma_b^2 \right) - \frac{\sigma_w^2}{2} \frac{k}{k+1} \frac{1}{\pi} \sqrt{q_h^{l-1}(x_1) q_h^{l-1}(x_2)}$$

B Derivation of the length and covariance map for RAI

For each node, one weight or the bias incoming to a neuron is replaced by a beta distribution random variable. Thus, the weights and bias are treated on an equal footing. To simplify the notations, we incorporate the bias in the weight matrix by introducing a fictitious additional node with a constant value of 1, i.e.,

$$\mathbf{s}^l(x) = [\phi(\mathbf{h}^l(x)), 1].$$

The evolution equation is now given by

$$\mathbf{h}^l(x) = \mathbf{W}^l \cdot \mathbf{s}^{l-1}(x).$$

It is easier to track the evolution using the activation instead of the pre-activations. So we define a few covariance matrices which will come in handy

$$q_s^l(x_1, x_2) = \frac{1}{N+1} \sum_{i=0}^N s_i^l(x_1) s_i^l(x_2)$$

$$q_{-k_j^l}^l(x_1, x_2) = \frac{1}{N} \sum_{t \neq k_j^l}^N s_t^l(x_1) s_t^l(x_2),$$

where k_j^l tags variables associated with the special weight. We will use the notations $q_s^l(x) = q_s^l(x, x)$ and $q_{-k}^l(x) = q_{-k}^l(x, x)$. The corresponding correlation coefficients are given by,

$$c_s^l(x_1, x_2) = \frac{q_s^l(x_1, x_2)}{\sqrt{q_s^l(x_1) q_s^l(x_2)}}$$

$$c_{-k_j^l}^l(x_1, x_2) = \frac{q_{-k_j^l}^l(x_1, x_2)}{\sqrt{q_{-k_j^l}^l(x_1) q_{-k_j^l}^l(x_2)}}$$

B.1 Derivation of the length map for RAI

Given $h^{l-1}(x)$, we can view $h_j^l(x)$ as

$$h_j^l(x) = \left(\sigma_w \sqrt{q_{-k_j^{l-1}}^{l-1}(x)} z + s_{k_j^{l-1}}^{l-1}(x) u \right),$$

where $z \sim \mathcal{N}(0, 1)$ and $u \sim \beta(2, 1)$. By applying the activation function and squaring it, we obtain

$$\phi(h_j^l(x))^2 = \phi \left(\sigma_w \sqrt{q_{-k_j^{l-1}}^{l-1}(x)} z + s_{k_j^{l-1}}^{l-1}(x) u \right)^2.$$

Next, we take an average over the weights and the special weight to get

$$\langle \phi(h_j^l(x))^2 | h^{l-1}(x) \rangle = \sum_{k_j^{l-1}=0}^N \frac{1}{N+1} \int dz du f(z) f(u) \phi \left(\sigma_w \sqrt{q_{-k_j^{l-1}}^{l-1}(x)} z + s_{k_j^{l-1}}^{l-1}(x) u \right)^2,$$

where $f(u) \sim \beta(2, 1)$ distribution, and $f(z) \sim \mathcal{N}(0, 1)$. We can take a sum over all nodes and re-write the equation in terms of the overlap

$$\langle q_s^l(x) | h^{l-1}(x) \rangle = \frac{1}{N+1} \left[1 + \sum_{j=1}^N \sum_{k_j^{l-1}=0}^N \frac{1}{N+1} \int dz du f(z) f(u) \phi \left(\sigma_w \sqrt{q_{-k_j^{l-1}}^{l-1}(x)} z + s_{k_j^{l-1}}^{l-1}(x) u \right)^2 \right]. \quad (5)$$

B.2 Derivation of the covariance map for RAI

The covariance map can be derived similarly, with a key difference of covariance between the pre-activations. For two input signals x_1 and x_2 , the covariance map reads

$$\begin{aligned} \langle q_s^l(x_1, x_2) | h^{l-1}(x_1), h^{l-1}(x_2) \rangle &= \frac{1}{N+1} \left[1 + \sum_{j=1}^N \sum_{k_j^{l-1}=0}^N \frac{1}{N+1} \int dz_1 dz_2 du f(z_1, z_2) f(u) \times \right. \\ &\times \left. \phi \left(\sigma_w \sqrt{q_{-k_j^{l-1}}^{l-1}(x_1)} z_1 + s_{k_j^{l-1}}^{l-1}(x_1) u \right) \phi \left(\sigma_w \sqrt{q_{-k_j^{l-1}}^{l-1}(x_2)} z_2 + s_{k_j^{l-1}}^{l-1}(x_2) u \right) \right], \end{aligned} \quad (6)$$

where $f(z_1, z_2)$ is the joint Gaussian distribution of z_1 and z_2 , with a covariance matrix given by

$$\Sigma_{k_j^l}^{l-1}(x_1, x_2) = \begin{bmatrix} q_{-k_j^{l-1}}^{l-1}(x_1) & q_{-k_j^{l-1}}^{l-1}(x_1, x_2) \\ q_{-k_j^{l-1}}^{l-1}(x_1, x_2) & q_{-k_j^{l-1}}^{l-1}(x_2) \end{bmatrix}.$$

We can re-write Eqn. 6 in terms of $c_{-k_j^l}^l(x_1, x_2)$

$$\begin{aligned} \langle q_s^l(x_1, x_2) | h^{l-1}(x_1), h^{l-1}(x_2) \rangle &= \frac{1}{N+1} \left[1 + \sum_j \sum_{k_j^{l-1}} \frac{1}{N+1} \int dz_1 dz_2 du f(z_1) f(z_2) f(u) \times \right. \\ &\times \left. \phi \left(\sigma_w \sqrt{q_{-k_j^{l-1}}^{l-1}(x_1)} z_1 + s_{k_j^{l-1}}^{l-1}(x_1) u \right) \times \right. \\ &\times \left. \phi \left(\sigma_w \sqrt{q_{-k_j^{l-1}}^{l-1}(x_2)} \left[c_{-k_j^l}^l(x_1, x_2) z_1 + \sqrt{1 - (c_{-k_j^l}^l(x_1, x_2))^2} z_2 \right] + s_{k_j^{l-1}}^{l-1}(x_2) u \right) \right], \end{aligned}$$

where $f(z_1) \sim f(z_2) \sim \mathcal{N}(0, 1)$ are standard Gaussian distributions. As suggested by Ref. [36], we can find the fixed point of the correlation map under the assumption that the length $q_h^l(x)$ has reached its fixed point. It is easy to see that $c_h^l(x_1, x_2) = 1$ is a fixed point of the correlation map.

C Stability of the fixed points for the length and correlation maps for RAI

C.1 Stability of the fixed point for the length map for RAI

The derivation of the analytical form of the length map (Eqn. 5) is difficult, and only bounds to the map have been derived [18]. Inspired by the analytical form of the length map for the anti-correlated initialization and the analysis done by Ref. [18], we assume that the length map has a linear dependence on $q_s^{l-1}(x)$. Under this assumption, we can find the stability of the fixed point of the length map by taking a derivative with respect to $q_s^{l-1}(x)$. Yet another problem exists. While taking a derivative, we have to encounter derivatives of the form

$$\frac{\partial s_{-k_j^{l-1}}^{l-1}(x)}{\partial q_h^{l-1}(x)}.$$

To simplify the calculations further, we employ a mean-field type approach by approximating $q_{-k_j}^l(x)$ by $q_s^l(x)$ and $s_{k_j}^l$ by its RMS value $q_s^l(x)$. Note that we can also approximate $s_{k_j}^l$ by its mean value, giving the same qualitative results. It simplifies Eqn. 5, and we obtain

$$\langle q_s^l(x) | h^{l-1}(x) \rangle = \frac{1}{N+1} \left[1 + (N+1) \int dz du f(z) f(u) \phi \left(\sqrt{q_s^{l-1}(x)} (\sigma_w z + u) \right)^2 \right].$$

To find the fixed point of the length map, we take a derivative wrt $q_s^{l-1}(x)$ to get the condition for stability of the fixed point $q^*(x)$. We denote the derivative by $\zeta_{q^*(x)}$. It separates the dynamics into two phases - a bounded phase when $\zeta_{q^*(x)} < 1$, and an unbounded phase when $\zeta_{q^*(x)} > 1$.

$$\begin{aligned} \zeta_{q^*(x)} &= \frac{\partial q_s^l(x)}{\partial q_s^{l-1}(x)} \Big|_{q_s^{l-1}(x)=q^*(x)} \\ \zeta_{q^*(x)} &= \frac{\partial}{\partial q_s^{l-1}(x)} \int dz du f(z) f(u) \phi \left(\sqrt{q_s^{l-1}(x)} (\sigma_w z + u) \right)^2 \\ \zeta_{q^*(x)} &= \frac{1}{\sqrt{q_s^{l-1}(x)}} \int dz du f(z) f(u) (\sigma_w z + u) \phi' \left(\sqrt{q_s^{l-1}(x)} (\sigma_w z + u) \right) \phi \left(\sqrt{q_s^{l-1}(x)} (\sigma_w z + u) \right) \\ \zeta_{q^*(x)} &= \sigma_w^2 \int dz du f(z) f(u) [\phi'(\sigma_w z + u)]^2 + \sigma_w \int dz du f(z) f(u) \phi'(\sigma_w z + u) \phi(\sigma_w z + u) \quad (7) \end{aligned}$$

where we have used the fact that for $a > 0$, $\phi(ax) = a \phi(x)$. On evaluating the integral, we find that $\zeta_{q^*(x)} = 1$ when $\sigma_w^2 = 0.56$. On comparing with the numerical results in Fig. 7, we find that this approximated result underestimates the critical point $\sigma_w^2 = 0.72$.

C.2 Stability of the fixed point for the correlation map for RAI

Under the assumption, $q_s^l(x) \rightarrow q^*(x)$, the correlation map has a fixed point $c_s^*(x_1, x_2) = 1$, and its stability can be calculated by the derivative of the correlation map evaluated at $c_s^{l-1}(x_1, x_2) = 1$. But again, we get into the difficulties mentioned in the previous section, and we employ the same assumptions to arrive at a tractable equation for the correlation map

$$\begin{aligned} \langle c_s^l(x_1, x_2) | h^{l-1}(x_1), h^{l-1}(x_2) \rangle &= \frac{1}{q_s^*(x)} \frac{1}{N+1} \left[1 + N \int dz_1 dz_2 du f(z_1) f(z_2) f(u) \times \right. \\ &\times \left. \phi \left(\sqrt{q_s^*(x)} (\sigma_w z_1 + u) \right) \phi \left(\sqrt{q_s^*(x)} \left[c_s^{l-1}(x_1, x_2) \sigma_w z_1 + \sqrt{1 - (c_s^{l-1}(x_1, x_2))^2} \sigma_w z_2 + u \right] \right) \right], \end{aligned}$$

Next, we take a derivative to get the condition for the stability of the fixed point $c_h^*(x_1, x_2) = 1$

$$\begin{aligned} \chi_1 &= \frac{\partial c_h^l(x_1, x_2)}{\partial c_h^{l-1}(x_1, x_2)} \Big|_{c_h^{l-1}(x_1, x_2)=1} \\ \chi_1 &= \frac{1}{q_h^*(x)} \frac{\partial}{\partial c_h^{l-1}(x_1, x_2)} \int dz_1 dz_2 du f(z_1) f(z_2) f(u) \phi \left(\sqrt{q_s^*(x)} (\sigma_w z_1 + u) \right) \times \\ &\times \phi \left(\sqrt{q_s^*(x)} \left[c_s^{l-1}(x_1, x_2) \sigma_w z_1 + \sqrt{1 - (c_s^{l-1}(x_1, x_2))^2} \sigma_w z_2 + u \right] \right) \Big|_{c_h^{l-1}(x_1, x_2)=1} \end{aligned}$$

$$\chi_1 = \sigma_w^2 \int dz du f(z) f(u) [\phi'(\sigma_w z + u)]^2. \quad (8)$$

The above equation is the same as the first term we obtained in the condition for the stability of the length map (Eqn. 7). We obtain a critical value of $\sigma_w^2 = 1.41$ by solving for $\chi_1 = 1$. We observe that the critical point for the length is smaller than the critical point of the correlation coefficient, and from our experience with ReLU networks with correlated weights, we expect RAI to have an ordered phase only, which is confirmed by numerical results (see Fig. 7).

D Derivation of length and correlation map for RAAI

D.1 Derivation for the length map for RAAI and the stability condition

For given $h^{l-1}(x)$, we can view $h_j^l(x)$ as

$$h_j^l(x) = \left(\sigma_w \sqrt{\tilde{q}^{l-1}(x)} z + s_{-k_j^{l-1}}^{l-1}(x) u \right),$$

where $\tilde{q}^{l-1} = q_{-k_j^{l-1}}^{l-1}(x) - \frac{k}{1+k} \left(m_{-k_j^{l-1}}^l(x) \right)^2$. Here $m_{-k_j^{l-1}}^l(x)$ is the mean value of $s_{-k_j^{l-1}}^{l-1}$ averaged over nodes in the previous layer. We can use the relation $(m_s^l(x))^2 = q_s^l(x)/\pi$ to re-define σ_w as

$$\tilde{\sigma}^2 = \sigma_w^2 \left(1 - \frac{k}{1+k} \frac{1}{\pi} \right),$$

which yields,

$$h_j^l(x) = \left(\tilde{\sigma} \sqrt{q_s^{l-1}(x)} z + s_{-k_j^{l-1}}^{l-1}(x) u \right),$$

Now, the entire analysis goes through as Section B.1, just with a re-definition of the variance. Now, we can read off the stability condition for the fixed point of the length map

$$\zeta_{q^*(x)} = \tilde{\sigma}_w^2 \int dz du f(z) f(u) [\phi'(\tilde{\sigma} z + u)]^2 + \tilde{\sigma} \int dz du f(z) f(u) \phi'(\tilde{\sigma} z + u) \phi(\tilde{\sigma} z + u) \quad (9)$$

On solving the equations numerically, we observe that the length is bounded when $\sigma_w^2 < 1.75$, which overestimates the numerical value observed numerically (see Fig. 8).

D.2 Derivation for the correlation map for RAAI and the stability condition

The derivation for the correlation map for RAAI can be done similar to RAI, with a key difference of the covariance matrix. The covariance matrix is given by

$$\Sigma_{k_j^l}^{l-1}(x_1, x_2) = \begin{bmatrix} q_{-k_j^{l-1}}^{l-1}(x_1) - \frac{k}{1+k} \left(m_{-k_j^{l-1}}^l(x_1) \right)^2 & q_{-k_j^{l-1}}^{l-1}(x_1, x_2) - \frac{k}{1+k} m_{-k_j^{l-1}}^l(x_1) m_{-k_j^{l-1}}^l(x_2) \\ q_{-k_j^{l-1}}^{l-1}(x_1, x_2) - \frac{k}{1+k} m_{-k_j^{l-1}}^l(x_1) m_{-k_j^{l-1}}^l(x_2) & q_{-k_j^{l-1}}^{l-1}(x_2) - \frac{k}{1+k} \left(m_{-k_j^{l-1}}^l(x_2) \right)^2 \end{bmatrix}.$$

Again, $c^*(x_1, x_2) = 1$ is a fixed point of the dynamics. On performing approximations as in Section C.2, we find that the stability condition is again given by Eqn. 8, which gives $\sigma_w^2 = 1.41$ as the phase transition boundary. Comparing it with Fig. 8, we find that it overestimates the critical value.

Note that instead of approximating $s_{k_j}^{l-1}$ by its RMS value $q_s^{l-1}(x)$, we can also approximate it by its mean value. In this case, we find that we overestimate all the boundaries. In Table 3, we compare the boundaries predicted by the RMS and mean approximations.

Approximation	$(\sigma_w^2)_q(RAI)$	$(\sigma_w^2)_c(RAAI)$	$(\sigma_w^2)_q(RAAI)$
RMS	0.57	1.41	1.75
Mean	0.85	1.46	1.89

Table 3: A comparison between the decision boundaries obtained by approximating $s_{k_j}^{l-1}$ by its RMS and mean value. The RMS approximation underestimates the length boundary for RAI, whereas it overestimates both the phase boundaries for RAAI. On the other hand, the mean approximation overestimates the phase boundaries for RAI and RAAI both.

E Code to generate weights drawn from RAAI distribution

```

1 import numpy as np
2
3 def RAAI(fan_in, fan_out, k = 100, variance_weights = 0.9):
4     """Randomized Asymmetric Anti-correlated Initializer (RAAI)
5     Arguments:
6     fan_in -- the number of neurons in the previous layer
7     fan_out -- the number of neurons in the next layer
8     corr -- correlation strength for the Gaussian weights
9     variance_weights -- variance of the weights
10    Returns:
11    W, b -- weight and bias matrices with shape(fan_in, fan_out), and (fan_out, )
12    """
13    corr = k/(1+k)
14    mean = np.zeros(fan_in + 1)
15    J = np.ones((fan_in + 1, fan_in + 1))
16    cov = (np.identity(fan_in + 1) - J*(corr/(fan_in + 1))) * variance_weights /
17    fan_in
18    P = np.random.multivariate_normal(mean = mean, cov = cov, size = (fan_out))
19    for j in range(P.shape[0]):
20        k = np.random.randint(0, high = fan_in + 1)
21        P[j, k] = np.random.beta(2, 1)
22    W = P[:, :-1].T
23    b = P[:, -1]
24    return W.astype(np.float32), b.astype(np.float32)

```